Journal of the Geological Society, London, Vol. **148,** 1991, pp. 541–548, 14 figs. Printed in Northern Ireland

Experimental evidence for water weakening of quartzite by microcracking plus solution–precipitation creep

S. W. J. DEN BROK & C. J. SPIERS

HPT Laboratory, Institute of Earth Sciences, Department of Geology, University of Utrecht, PO Box 80.021, 3508 TA Utrecht, The Netherlands

Abstract: Natural quartzites have been experimentally deformed at a temperature of 1073 K, a confining pressure of 1.2 ± 0.1 GPa, strain rates of 10^{-5}, 10^{-6} and $10^{-7}\,s^{-1}$ and in the presence of 0.4 wt% of added water. Microstructures after deformation indicate that at strain rates of 10^{-5}–$10^{-6}\,s^{-1}$ crystal plastic deformation is predominant. This is evident from abundant deformation lamellae in the original grains, and the fact that these grains show a (weak) crystallographic preferred orientation. New grains are absent or of relatively minor volumetric importance. In contrast, samples deformed at $10^{-7}\,s^{-1}$ show numerous arrays of fine, new polygonal to euhedral quartz grains developed in axially aligned transgranular and grain boundary microcracks. These new-grain aggregates are characterized by abundant microscale voids, fine intergranular channels and fluid inclusion trails. Syntaxial overgrowth structures on crack walls are also widespread. The aggregates of new grains are thus interpreted to have formed by precipitation from solution. In addition, old grain boundaries oriented perpendicular to the shortening direction show evidence for dissolution. The old grains show almost no deformation lamellae, subgrains or *c*-axis preferred orientation. It therefore appears that at strain rates of $10^{-7}\,s^{-1}$ microcracking and solution-precipitation creep are the dominant deformation mechanisms.

Experimental deformation studies on natural single crystals of quartz and on natural quartzite, have shown that small amounts of added water can considerably reduce the flow strength in comparison with the behaviour of dry material (e.g. for data on natural single crystals see Kronenberg *et al.* 1986, Ord & Hobbs 1986; for data on natural polycrystals see Jaoul *et al.* 1984, Kronenberg & Tullis 1984, Mainprice & Paterson 1984, Koch *et al.* 1989). This phenomenon, commonly referred to as 'hydrolytic weakening' or 'water weakening', is widely believed to result from intracrystalline effects such as a reduction in Peierls stress for glide, promotion of climb, or enhanced dislocation multiplication, these being caused by water-related defects penetrating the quartz lattice. Despite the considerable amount of work done on the subject, however, it must be admitted that the mechanism by which water weakening occurs remains poorly understood (see Koch *et al.* 1989; Paterson 1989).

The present paper reports a detailed microstructural study of natural quartzites, deformed experimentally in a Griggs solid-medium apparatus at a temperature of 1073 K, at a confining pressure of 1.2 GPa, at strain rates of 10^{-5}, 10^{-6} and $10^{-7}\,s^{-1}$, and with 0.4 wt% of added water. The observations indicate that at the lowest strain rates, microcracking and solution-precipitation creep are the dominant deformation mechanisms and cause a significant weakening effect. The results cast doubt on the widely accepted idea that water weakening seen in experimental deformation of quartzites is an intracrystalline process.

Starting material

All experiments were performed on Dongelberg quartzite (Fig. 1) from the Cambrian of the Brabant Massif (Belgium). This is a very dense material (porosity $< 0.1\%$) consisting of *c.* 97 vol% quartz with a mean grain size of 150–250 μm. The quartz grains are equant to irregular in shape and define a very weak grain shape preferred orientation parallel to the bedding. They show undulatory extinction in bands (in about 50% of the grains) oriented predominantly parallel to the *c*-axes. The material has a very weak crystallographic preferred orientation (Fig. 1a). Grain boundaries are irregular or serrated showing grain boundary bulges characteristic of grain boundary migration. Locally, grain boundaries contain finer polygonal quartz grains (20–60 μm) as well as phengitic mica platelets (1–2 vol%), up to 30 μm long, aligned parallel to the boundary. Fine-grained (<5 μm) Fe-hydroxides (1–2 vol%) at the grain boundaries give the bulk sample a brownish colour. Fluid inclusions occur along grain boundaries or deformation band boundaries but are of very minor volumetric importance (<2 μm diameter; <0.1 vol% in total). Healed microcracks are present but rare. The water content, determined by measuring the weight loss of samples heated for 30 hours in nitrogen gas at 800 °C, is about 0.3% (including the water made available from dehydration of micas and Fe-hydroxides).

Experimental procedure and data processing

Cylindrical samples measuring 6 mm in diameter by 12 ± 1 mm in length were cored from a single block of the Dongelberg quartzite at 45° to the bedding. This was done using a diamond coring tool with water as lubricant. The ends of the samples were ground flat and parallel to within 30 μm measured parallel to the sample length. The specimens were subsequently oven-dried at 150 °C for 12 hours, and then weld-sealed in gold jackets (400 μm wall thickness) together with 3–4 mg (0.4 wt%) of distilled water. In the jacketing procedure, one end of the tubular jacket was first formed into a cone-shaped closure (see Fig. 2) by turning on a lathe. The tip of the resulting cone was sealed with an argon precision arc welder. The water was then placed in the capsule (i.e. into the cone shaped pit), followed by the sample. While the water was immobilized by freezing in a stream of liquid nitrogen played onto the sealed cone,

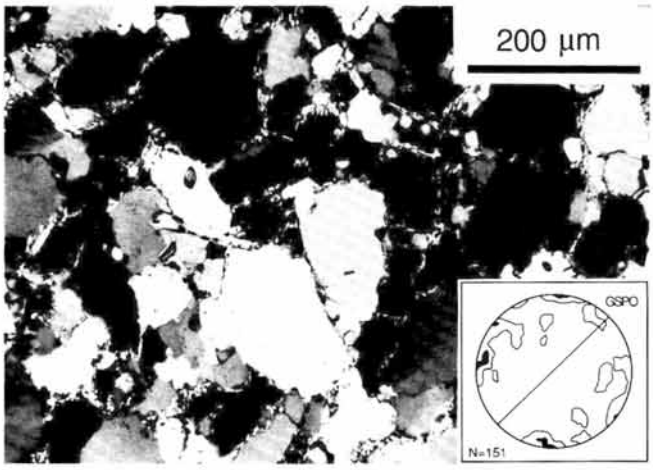

(a)

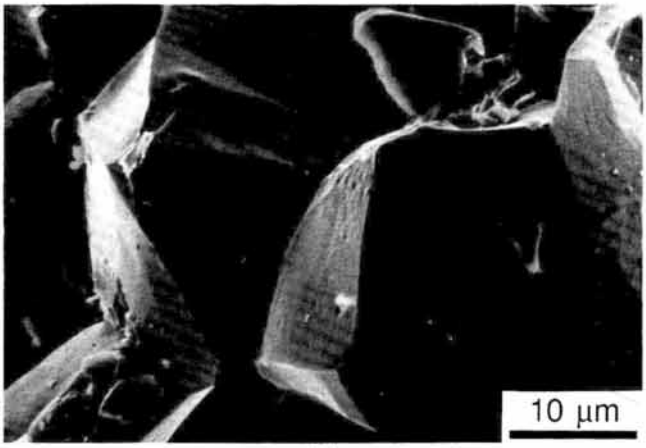

(b)

Fig. 1. (**a**) Optical micrograph (crossed polars) of starting material (Dongelberg quartzite) and diagram showing the weak initial *c*-axis preferred orientation (1% contour intervals). The weak grain shape preferred orientation is indicated (GSPO). This is parallel to bedding.
(**b**) Secondary electron image of starting material.

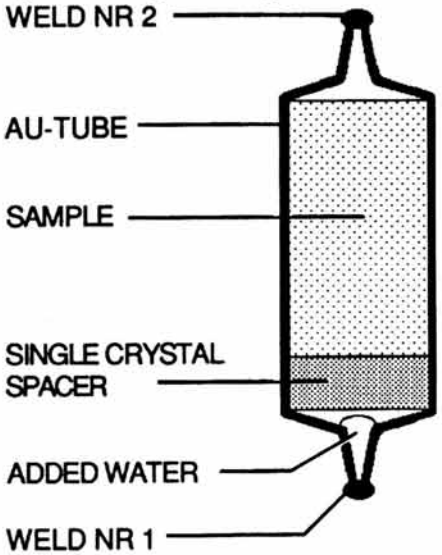

Fig. 2. Schematic diagram of encapsulated sample prior to deformation (not to scale). The single crystal spacer was added in experiment GRU23 only.

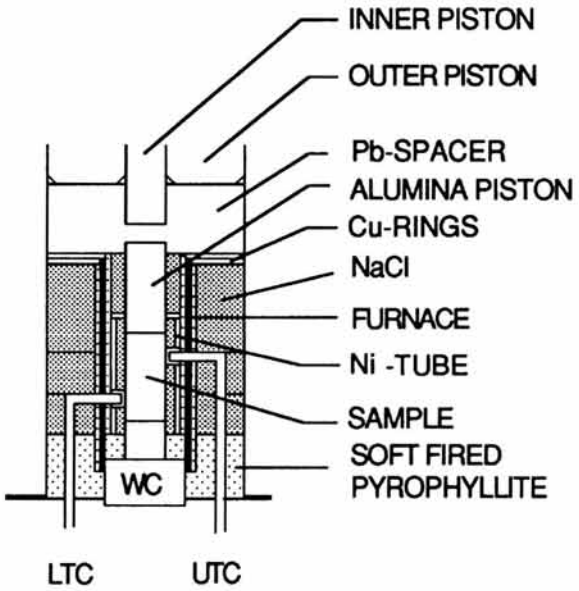

Fig. 3. Sample assembly (not to scale). Upper and lower thermocouples denoted UTC and LTC.

the open end of the capsule was formed into a second cone and subsequently weld-sealed. Both ends were then carefully flattened using a hand press. Lastly, the capsules were tested for leaks by immersion in oil at 120 °C.

Deformation experiments were conducted in a Tullis-modified Griggs apparatus with NaCl as the confining medium. The sample assembly used is shown in Fig. 3. The samples were heated using a graphite resistance furnace and temperatures were measured and controlled using two Pt-Pt10%Rh thermocouples. Temperature gradients were minimized by surrounding the sample with a Ni-tube (700 μm wall thickness). Temperature, pressure (in the confining pressure ram), axial load and displacement signals were continuously monitored during the experiment using a chart recorder and PC-based data logger.

In setting up each test, temperature and pressure were raised simultaneously in order to follow the water isochore of 1 g cm^{-3} as closely as possible. The experiments were performed in constant displacement rate mode at 1073 K and at 1.2 ± 0.1 GPa confining pressure. The imposed strain rates ($\dot{\varepsilon}$) were 1.1×10^{-5}, 1.1×10^{-6} and 1.1×10^{-7} s^{-1}. The total strains achieved fell in the range 5 to 40%. After deformation, the piston was moved upwards at maximum speed (3×10^{-3} mm s^{-1}), and the temperature and pressure were lowered, once again following the water isochore of 1 g cm^{-3} as closely as possible. Cooling times varied from 1–50 minutes. For purposes of comparison, one sample was deformed without added water at 10^{-7} s^{-1} under otherwise similar experimental conditions. Two samples were hydrostatically loaded only. These were maintained at 1073 K and 1.2 ± 0.1 GPa for 90 and 113 hours respectively. Twelve experiments were carried out in all (see Table 1).

With regard to the processing of the raw data it is important to note that the measured axial displacement and load were corrected for apparatus distortion (at 1073 K and 12 GPa) and for friction respectively. Differential stresses were calculated using the initial cross section of the samples. Axial strain was computed with respect to the sample length at ambient (NTP) conditions. The resolution of the stress measurement is believed to be approximately 25 MPa, a figure which is closely comparable with that obtained in previous work using the Griggs apparatus (e.g. Jaoul *et al.* 1984).

Table 1. *Summary of experimental data*

Sample number		Strain rate (s^{-1})	Finite strain (%)	P_c (MPa)	LTC (°C)	UTC (°C)	t_1 (h:m)	t_2 (h)	t_3 (h:m)	Yield stress (MPa)
GRU15	wet	—	—	1100	805	800	1:50	113	0:40	—
GRU19	wet	—	—	1250	764	800	6:20	90	1:30	—
GRU13	wet	1.1×10^{-5}	12.3	1040	793	815	4:10	13	0:50	613
GRU14	wet	1.1×10^{-5}	5.5	1060	802	802	5:40	23	0:30	591
GRU10	wet	1.1×10^{-6}	8.6	1060	786	810	8:10	38	5:00	152
GRU20	wet	1.1×10^{-6}	12	1240	802	800	3:50	88	0:50	—
GRU21	wet	1.1×10^{-6}	6.3	1240	806	800	5:20	49	0:40	—
GRU29	wet	1.1×10^{-6}	40	1160	784	810	26:50	32	0:01	187
GRU11	wet	1.1×10^{-7}	10.9	1040	784	800	2:20	19	2:40	<25
GRU23*	wet	1.1×10^{-7}	10.7	1140	760	800	26:30	70	0:26	<25
GRU26	wet	1.1×10^{-7}	13.5	1130	798	800	4:30	144	0:20	<25
GRU31	dry	1.1×10^{-7}	9.5	1160	776	800	21:10	78	0:50	137

GRU15 and GRU19 are samples hydrostatically loaded only. Wet, 0.4 wt% water added; dry, as-received, deformed without added water; P_c, confining pressure; LTC, lower thermocouple temperature; UTC, upper thermocouple temperature; t_1, elapsed time to reach *PT* conditions; t_2, time at *PT* conditions before deformation; t_3, elapsed time after deformation to reach room *PT* conditions.

* Sample deformed with single crystal spacer (see Fig. 2).

Mechanical results

The mechanical data obtained from the present tests are shown in the form of differential stress versus axial strain curves in Fig. 4. At a strain rate ($\dot{\varepsilon}$) of $10^{-7}\,s^{-1}$, the differential stress supported by the wet-deformed samples (GRU11, 23, 26) was too low to measure, i.e. no detectable increase in axial load occurred at the calculated hitpoint of the upper piston against the sample. In contrast, the sample deformed at $10^{-7}\,s^{-1}$ without added water (GRU31), showed macroscopic yield behaviour followed by strain hardening. Most samples deformed wet at 10^{-5} and $10^{-6}\,s^{-1}$ also exhibited macroscopic yield behaviour, followed by strain hardening in some cases and softening in others. Steady state deformation was not seen in any of the experiments. Nonetheless, the flow stresses measured after macroscopic yield (where observed) are plotted versus strain rate in the log–log plot of Fig. 5. This shows that if power law creep behaviour is assumed (regardless of mechanism, and assuming that the mechanical data reflect sample behaviour), a stress exponent $n < 1.3$ is implied for the region $\dot{\varepsilon} < 10^{-6}\,s^{-1}$.

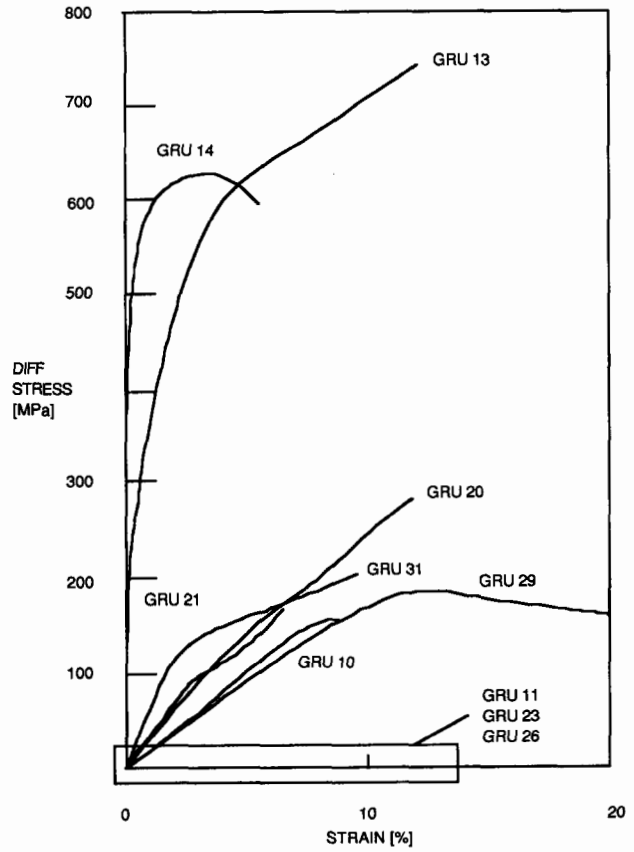

Fig. 4. Stress/strain curves obtained from the present experiments. The curves of samples deformed wet at $10^{-7}\,s^{-1}$ lie within the indicated box, i.e. they were below the stress resolution limit of approximately 25 MPa.

Microstructural observations

The microstructure of the Dongelberg quartzite has already been described under the heading 'starting material'. Samples which were hydrostatically loaded only (GRU15, 19) show only minor microstructural modifications, namely small numbers of through-going cracks (on the sample scale) inclined at 0–20° to the sample long axis. Some of these cracks show shear offsets up to about 300 μm. Locally the cracks are healed, or filled with very fine inequant quartz grains (<5 μm). Small numbers of healed, grainscale (transgranular) microcracks were also observed. These microcracks are marked by fluid inclusions (<2 μm) and are axial in orientation. Locally they separate areas of slightly different optical extinction, i.e. there is a minor crystallographic misorientation developed across the crack walls.

By contrast, the experimentally deformed samples show substantial modification of the starting microstructure. Two distinct microstructural signatures are developed.

(1) Samples deformed wet at 10^{-5} (GRU13 & 14) and without added water at $10^{-7}\,s^{-1}$ (GRU31). In these samples

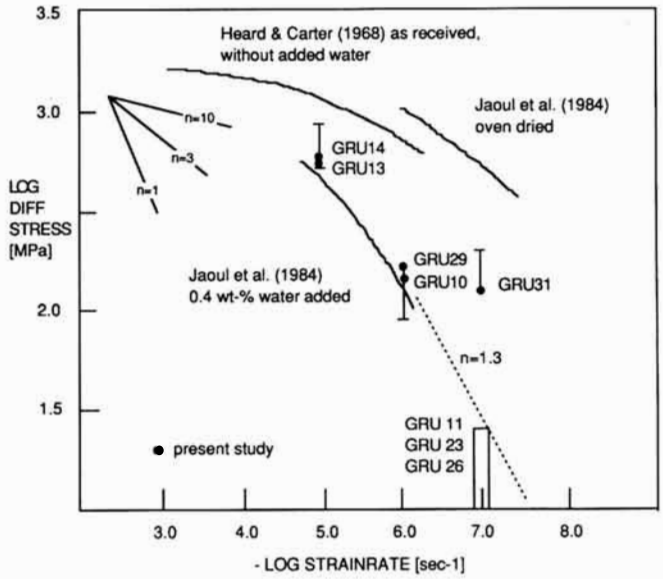

Fig. 5. Log–log plot of differential stress versus strain rate constructed from the stress strain curves of Fig. 4. Solid circles and range bars refer respectively to the macroscopic yield points obtained in the present experiments (where observed) and the range of flow stresses recorded after yield. The differential stresses supported by samples deformed wet at $10^{-7}\,s^{-1}$ lie within the indicated box or lower. Solid curves represent the data of Heard & Carter (1968; 800 °C, 0.8 GPa confining pressure, deformed as received without added water in a gas apparatus) and of Jaoul *et al.* (1984; 800 °C, 1.5 GPa confining pressure, deformed oven dried with and without 0.4 wt% added water in a Griggs solid medium apparatus).

deformation bands and undulatory extinction features are present in almost all the grains. A minor grain flattening fabric is also apparent in samples deformed at higher strains (Fig. 6). Furthermore, 60–80% of the original grains contain deformation lamellae (Fig. 6; note that deformation lamellae were not observed in the starting material). The lamellae occur dominantly at 45° to the shortening direction, they are mostly subbasal in orientation, and were always observed to lie more or less perpendicular to the experimentally produced deformation bands.

(2) Samples deformed wet at $10^{-7}\,s^{-1}$ (GRU11, 23 & 26). In these samples, very few (<5%) of the original grains contain deformation lamellae, and the frequency of deformation bands and undulatory extinction features only slightly exceeds that of the starting material. The experimentally produced microstructure is instead characterized by conspicuous intergranular arrays of fine, new, polygonal to euhedral quartz grains (5–50 μm). These arrays are preferentially aligned parallel to the shortening direction and locally cross-cut the older grains (Figs 7, 8 & 9). No evidence was found for any intracrystalline deformation features (i.e. deformation lamellae or bands) in these new grains. The arrays contain abundant microcavities or voids (<10 μm; *c.* 1 vol% in all; Fig. 10), intergranular channel structures and fluid inclusions trails. The void-bounded surfaces of new grains are mostly euhedral whereas new grain boundaries (i.e. grain-to-grain boundaries) are heavily decorated with fluid inclusions. Phengitic micas (1–50 μm) and fine-scale (<1 μm) Fe-bearing crystalline efflorescences also grow within the new grain arrays. Old grain boundaries

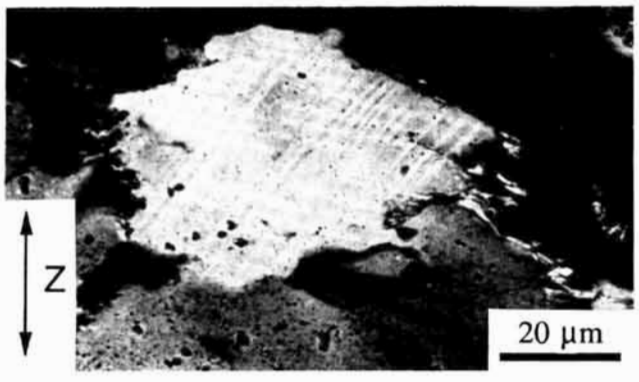

Fig. 6. Optical micrograph of experimentally produced deformation lamellae in sample GRU31, deformed as received without added water at $10^{-7}\,s^{-1}$ (crossed polars). Note grain flattening.

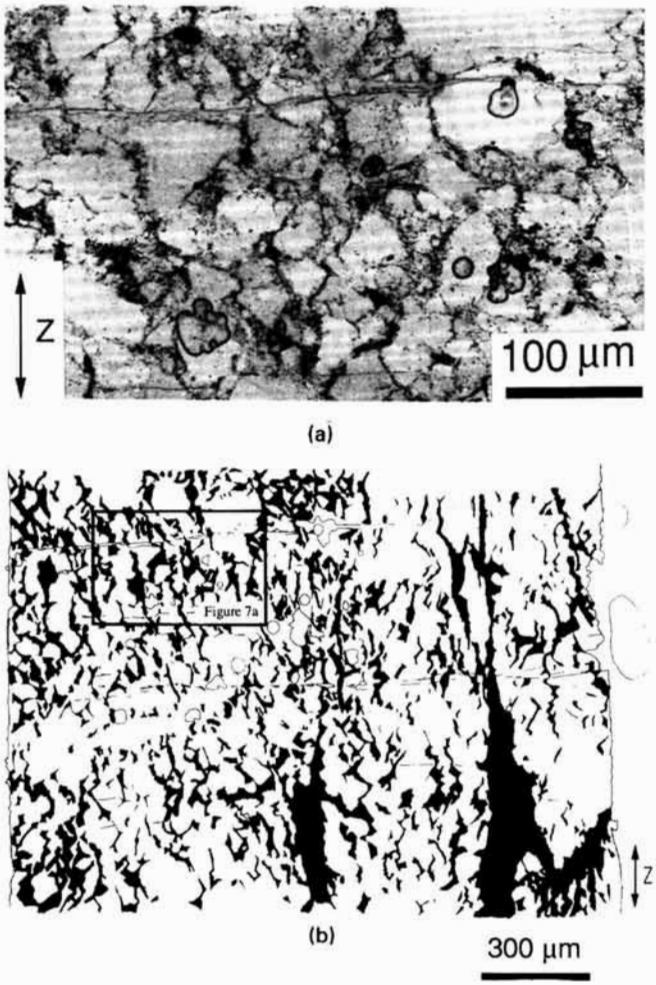

Fig. 7. (**a**) Optical micrograph (plane polarized light) of sample GRU11 (wet, $10^{-7}\,s^{-1}$) showing intergranular arrays of fine new quartz grains developed parallel to the shortening direction (Z). (**b**) Traced micrograph showing the distribution of arrays of new grains (in black) in sample GRU11. Note preferential orientation parallel to Z. Black areas do not necessarily represent sites of precipitation only, but also sites of microcracking. Note also that apparently wide black areas may reflect oblique sectioning (30 μm section). Horizontal cracks are (un)loading cracks. Location of Fig. 7a is indicated.

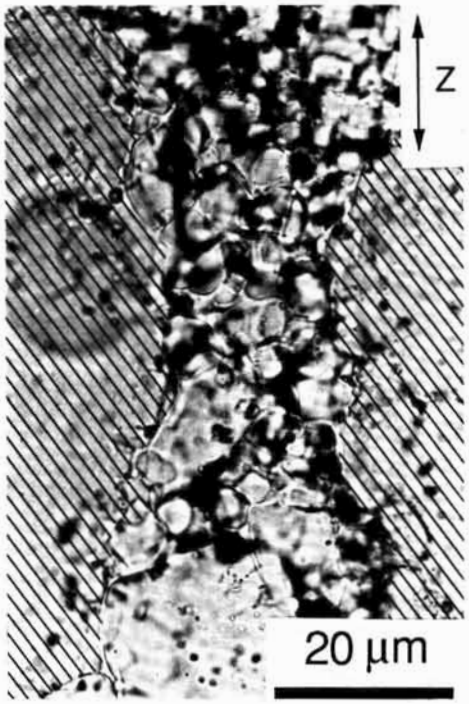

Fig. 8. Optical micrograph of arrays of new fine-grained quartz grains preferentially aligned parallel to the shortening direction (Z). Sample: GRU11 deformed with added water at $10^{-7}\,s^{-1}$. Note the abrupt transition from old to new grains and the euhedral shape of many of the new quartz crystals (plane polarized light). Old grains as identified on the optical microscope rotation stage are hatched. In some cases the old grains separated by new grain arrays have similar crystallographic orientation, suggesting transgranular fracture.

oriented parallel to the shortening direction are often dilated and show (sub)euhedral, syntaxial overgrowth structures (Fig. 11). These frequently appear pinned by micas, and fluid inclusion trails separating distinct (syntaxial) overgrowth cells are common. Some old grains appear to be slightly flattened and exhibit mica 'beards' growing perpendicular to the shortening direction (Z). The

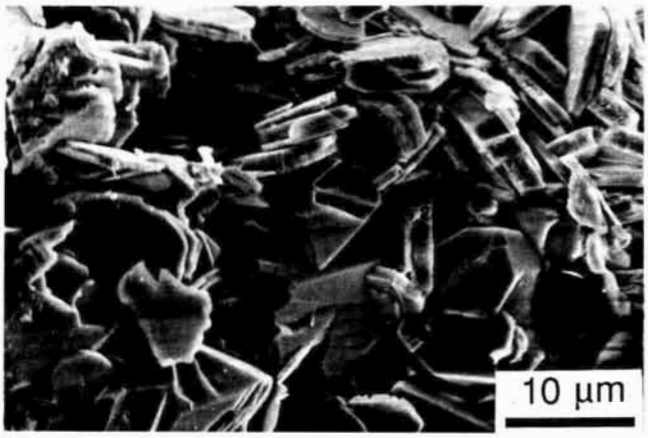

Fig. 9. Secondary electron images of grain boundary arrays of quartz grains in sample GRU11 (wet, $10^{-7}\,s^{-1}$). Note sub- to euhedral morphology, voids, and mica platelets included in the quartz.

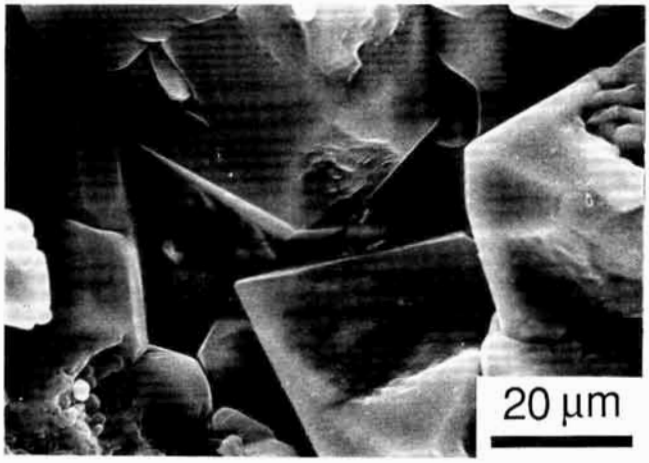

Fig. 10. Secondary electron image of aggregates of new grains in sample GRU11 (wet, $10^{-7}\,s^{-1}$) showing the presence of microcavities and growth features.

old grains also show numerous straight, healed intra- and transgranular microcracks aligned parallel to Z. Locally, the walls of intra- and transgranular microcracks show euhedral crystal morphology, again resembling syntaxial overgrowths. Old grain boundaries oriented perpendicular to Z show abundant fluid inclusions occupying up to 25% of the boundary surface. However, the overgrowth features seen on dilated grain boundaries oriented parallel to Z are conspicously absent. In experiment GRU23, the originally polished surface of a quartz single crystal spacer, placed in the sample capsule between sample and piston, revealed well developed indentations (50–200 μm in diameter) corresponding to grains in the quartzite sample. These indentations are characterized by irregular channel structures and abundant fluid inclusions similar to those seen on grain boundaries oriented perpendicular to Z in the bulk sample (Fig. 12). In the quartz spacer, numerous healed microcracks were visible as fluid inclusion trails oriented parallel to Z. The intervening regions are slightly misoriented (<3°). Optically, the single crystal spacer showed no evidence for crystal plastic deformation.

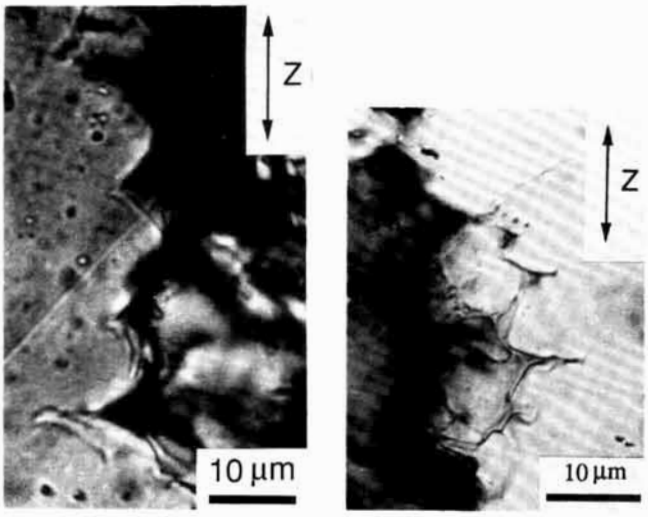

Fig. 11. Optical micrographs of syntaxial overgrowths of quartz at grain boundaries parallel to the shortening direction (Z) in sample GRU11 (wet, $10^{-7}\,s^{-1}$) (crossed polars).

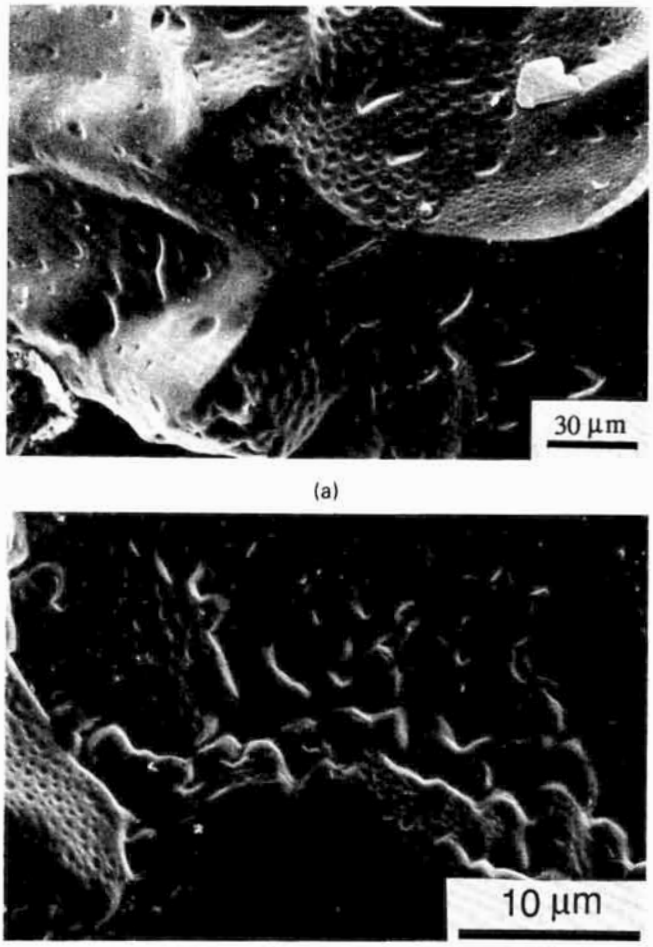

Fig. 12. Secondary electron images of the originally polished surface of the quartz single crystal spacer oriented perpendicular to Z in experiment GRU23 (wet, $10^{-7}\,s^{-1}$). Note the well-developed indentations with (**a**) fluid inclusions and (**b**) irregular channel structures.

Samples deformed wet at intermediate strain rates, i.e. at $10^{-6}\,s^{-1}$, typically show both types of microstructure described above (Fig. 13). Deformation lamellae were observed in *c.* 50% and *c.* 85% of the grains in GRU10 and GRU29 respectively. It is important to note that the optically estimated bulk fluid density of the fluid observed in the inclusions in all water-added samples (whether deformed or undeformed) is approximately 0.8 (volume of liquid divided by total volume). This indicates that fluid pressures during the development of these inclusions were close to the imposed confining pressure (at 1073 K and 1.1 GPa the density of water is approximately 0.9).

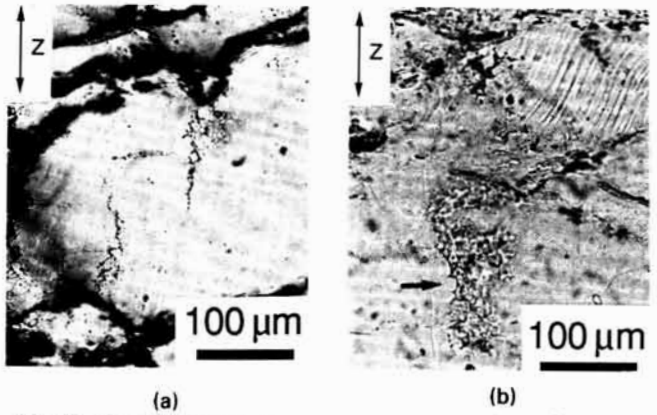

Fig. 13. Optical micrographs of sample GRU29 deformed wet at $10^{-6}\,s^{-1}$ showing (**a**) microcracks with syntaxial overgrowth at crack walls and (**b**) deformation lamellae together with aggregates of new grains and overgrowth structures (see arrow).

C-axes preferred orientations

Quartz *c*-axes orientations have been measured optically in the starting material, in the hydrostatically loaded samples, and in the axially deformed samples. Both the starting material and the hydrostatically loaded samples show a weak peripheral double maximum with a relatively pole-free area in the foliation (i.e. bedding) plane (Figs 1a & 14a). Samples deformed in the presence of added water at $10^{-6}\,s^{-1}$, and without added water at $10^{-7}\,s^{-1}$, also show a peripheral double maximum. In these cases, however, the maxima are more pronounced and are symmetrically disposed with respect to the experimentally imposed deformation geometry (Fig. 14b, c & d). Old grain *c*-axes in

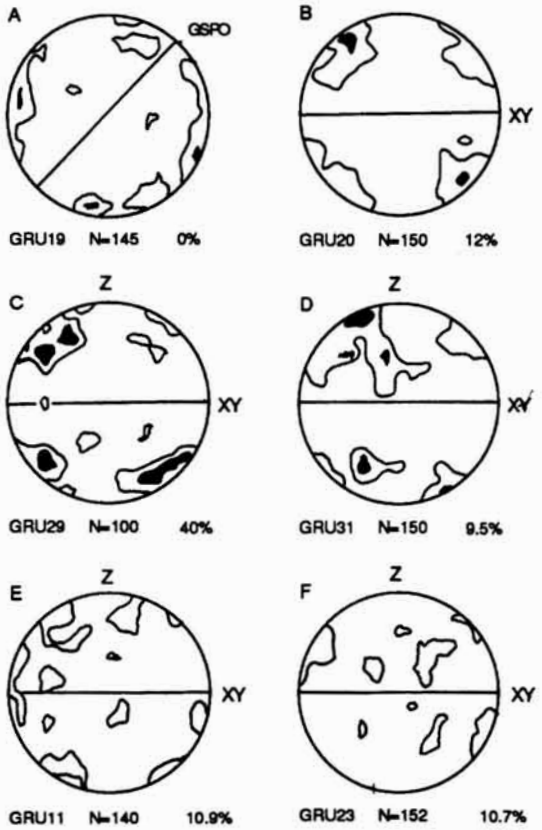

Fig. 14. Optically measured *c*-axes pole figures with 1% density contour intervals. XY-plane of experimentally imposed flattening is indicated. (**a**) Starting material after hydrostatic loading only, at 1073 K (sample GRU19; GSPO, initial grain shape preferred orientation, parallel to bedding). (**b**) & (**c**) *c*-axes of original grains in samples deformed wet at $10^{-6}\,s^{-1}$ (GRU20 and GRU29 respectively). (**d**) Original grains in sample GRU31 deformed without added water at $10^{-7}\,s^{-1}$. (**e**) & (**f**) Original grains of samples deformed with added water at $10^{-7}\,s^{-1}$ (GRU11 and GRU23 respectively). N.B. All samples were compressed at 45° to initial grain shape fabric. Axial strains are indicated in %.

the samples deformed wet at $10^{-7}\,s^{-1}$ show only a very weak preferred orientation (Fig 14e & f) which appears unrelated to the deformation symmetry.

Interpretation of results

It is shown above that samples deformed wet at strain rates of 10^{-5} and $10^{-6}\,s^{-1}$, plus those deformed without added water at $10^{-7}\,s^{-1}$, exhibit convincing microstructural evidence for crystal plastic deformation. Deformation lamellae and deformation bands are well developed in the old grains and a weak crystallographic and shape preferred orientation is produced. Since the lamellae formed in the dry samples as well as in the wet ones, the presence of added water does not seem to be essential for their formation.

In contrast, the water-weakened samples deformed at $10^{-7}\,s^{-1}$ (and to a lesser extent at $10^{-6}\,s^{-1}$) show microstructures that are clearly related to the presence of the added water. This is inferred from the numerous microcavities, fluid inclusions and intergranular channel structures present in the observed arrays of new (sub)euhedral quartz and mica grains. These axially aligned arrays of new grains were not present in the starting material. They are interpreted to result from precipitation from solution in grain boundary and transgranular microcracks aligned parallel to the shortening direction. In addition, indentations (without plastic deformation) into the polished surface of the quartz single crystal included in experiment GRU23 (see Fig. 2) provide strong evidence that pressure solution took place in the wet tests at $10^{-7}\,s^{-1}$ (note also the absence of overgrowth features on the grain boundaries oriented normal to the shortening direction). In all samples deformed under these conditions, the old grains are more or less free of subgrains, deformation lamellae, and crystallographic preferred orientation (weaker than in starting material). These observations indicate that crystal plastic deformation did not significantly contribute to the development of the microstructure. It is concluded that in wet material, at $10^{-7}\,s^{-1}$, microcracking and solution-precipitation processes were responsible for most of the deformation, at least for finite strains up to about 14%. The very low stress exponent ($n < 1.3$) inferred from Fig. 5 for wet samples at $\dot{\varepsilon} < 10^{-6}\,s^{-1}$ is consistent with this conclusion, though more reliable mechanical data are clearly desirable.

Comparison with previous experiments

Comparison of experimental data obtained in different laboratories is complicated by the use of different starting materials, deformation apparatus, sample assemblies, water fugacities, fluid pressures and chemistries, confining pressures, temperatures and strain rates. Only the experimental study of Jaoul *et al.* (1984) seems directly comparable with the present experiments. However, it is important to note that the microstructures and weakening behaviour reported by these authors is broadly similar to those observed in other experimental studies on quartzites (e.g. Tullis *et al.* 1973; Parrish *et al.* 1976; Kronenberg & Tullis 1984; Koch *et al.* 1989). Jaoul *et al.* (1984) used Heavitree quartzite (grain size *c.* 150 μm) as a starting material with varying amounts ($\leq$0.5 wt%) of added water. Their tests were performed at 1.5 GPa confining pressure, temperatures of 1073 to 1373 K and strain rates varying from 10^{-4}–$10^{-7}\,s^{-1}$.

The steady-state rheological data obtained by Jaoul *et al.* (1984) at 1073 K, with an H_2O content of 0.4 wt%, seem broadly consistent with the flow stress versus strain rate data reported in this study (see Fig. 5), and likewise show water weakening at low strain rates with power law stress exponents reaching values as low as 1.4 or even 1.2 (Jaoul *et al.* 1981). The microstructures reported by Jaoul *et al.* (1984) for water-weakened material also seem to be very similar to the solution transfer plus infilled crack microstructure seen in the present experiments on wet material at $10^{-7}\,s^{-1}$ (see fig. 3E, Jaoul *et al.* 1984, cf. present Fig. 7a). However, Jaoul *et al.* (1984) interpret this microstructure as indicative of crystal plasticity plus dynamic recrystallization (core and mantle structure). They correlate their water weakening effect with the onset of this latter process and suggest that weakening is actually caused by intracrystalline enhancement of climb and glide by dissolved water defects ('classical' hydrolytic weakening argument).

This interpretation would imply that water weakening should be time dependent due to progressive penetration of water into the original grains (1–10 μm per 24 hours, after Kronenberg *et al.* 1986). However, no progressive change in creep behaviour with time has been observed (Jaoul *et al.* 1984; Kronenberg & Tullis 1984). Furthermore, Kronenberg & Wolf (1990) report that the intergranular water content of water-weakened Heavitree quartzite appears unchanged before and after experimental deformation.

On the basis of the above information, it is proposed here that the water weakening effect reported by Jaoul *et al.* (1984) was very probably due to the same process as that observed in the present experiments, i.e. due to coupled microfracture plus solution-precipitation transfer. Additional support for the operation of this type of mechanism under the present or similar conditions, as well as those of Jaoul *et al.* (1984), is widespread in the literature. For example, extensional pockets of 'recrystallized' grain boundaries parallel to σ_1 are also reported by Dell'Angelo & Tullis (1989). These pockets contain segregations of impurities and very small amounts of melt and were interpreted as an extensional crenulation cleavage (though, as pointed out by the authors, they do not appear to crenulate a foliation). In addition, ample evidence has been reported in the literature for the existence of interconnected grain boundary fluids, microvoids, and channel structures under similar conditions to those investigated here (for hydrostatic experiments see Watson & Brenan 1987, Mackwell & Weathers 1987, Mackwell *et al.* 1989; for non-hydrostatic experiments see Den Brok 1989, Karato & Masuda 1989, Mackwell *et al.* 1989).

In the case of experiments on single crystals, there can be little doubt that a truly intracrystalline water weakening effect occurs in wet synthetic quartz. However, in experiments on dry natural crystals tested with added water, substantial evidence has been reported for a correlation between weakening and microcracking (Kirby & Kronenberg 1984; Kronenberg *et al.* 1986; Fitz Gerald *et al.* 1987). In these cases, however, it still remains unclear whether microcracking itself is associated with the weakening (possibly in association with solution transfer processes), or that it simply reduces the diffusion path for water into the crystal, thus allowing intracrystalline weakening effects to take place (Ord & Hobbs 1987).

Conclusion

The present experiments indicate that at 1073 K and 1.2 GPa confining pressure, at a strain rate of $10^{-7}\,s^{-1}$ (and to a lesser extent also at $10^{-6}\,s^{-1}$), water weakening of Dongelberg quartzite is achieved by microcracking and solution-precipitation creep, rather than by any intracrystalline effect. This casts doubt on the widely accepted idea that water weakening of quartzites seen in experiments is due to an intracrystalline hydrolytic weakening mechanism (see also Den Brok 1989; Mackwell *et al.* 1989). To resolve this question, further systematic work is clearly needed, using standardized starting materials, standardized experimental set-ups and conditions, and using controlled and/or measured pore fluid pressures and water fugacities.

We are indebted to J. Urai for work put into setting up the Griggs apparatus at Utrecht, for use of the sample assembly which he designed and the time spent in teaching SWJ den B how to work with the Griggs machine. R. Bakker, H. de Bresser, C. Peach and R. Vissers are thanked for their comments on the initial manuscript. The investigations were supported by the Netherlands Foundation for Earth Science Research (AWON) with financial aid from the Netherlands Organization for Scientific Research (NWO).

References

DELL'ANGELO, L. N. & TULLIS, J. 1989. Fabric development in experimentally sheared quartzites. *Tectonophysics*, **169**, 1–21.

DEN BROK S. W. J. 1989. The effect of water on the experimental deformation of natural quartzite: evidence for diffusional creep. *Terra abstracts*, vol. 1, nr. 1, EUG V, Strasbourg, 20–23 March 1989, 377.

FITZ GERALD, J. D., ORD, A., BOLAND, J. N. & MCLAREN, A. C. 1987. The water-weakening effect in experimental deformation of quartz. *International Conference on Deformation of Crustal Rocks, Geological Society of Australia, Abstracts*, **19**, 68.

HEARD, H. C. & CARTER, N. L. 1968. Experimentally induced "natural" intragranular flow in quartz and quartzite. *American Journal of Science*, **266**, 1–42.

JAOUL, O., SHELTON, G. & TULLIS, J. 1981. Quartzite deformation as a function of water at 15 Kb: Preliminary results. *EOS AGU Transactions*, **62**, 396.

——, TULLIS, J. & KRONENBERG, A. K. 1984. The effect of varying water contents on the creep behaviour of Heavitree quartzite. *Journal of Geophysical Research*, **89**, 4298–4312.

KARATO, S. & MASUDA, T. 1989. Anisotropic grain growth in quartz aggregates under stress and its implication for foliation development. *Geology*, **17**, 695–698.

KIRBY, S. H. & KRONENBERG, A. K. 1984. Hydrolytic weakening of quartz: uptake of molecular water and the role of microfracturing. *EOS AGU Transactions*, **65**, 277.

KOCH, P. S., CHRISTIE, J. M., ORD, A. & GEORGE, R. P., JR. 1989. Effect of water on the rheology of experimentally deformed quartzite. *Journal of Geophysical Research*, **94**, 13975–13996.

KRONENBERG, A. K. & TULLIS, J. 1984. Flow strengths of quartz aggregates: grain size and pressure effects due to hydrolytic weakening. *Journal of Geophysical Research*, **89**, 4281–4297.

—— & WOLF, G. H. 1990. Fourier transform infrared spectroscopy determinations of intragranular water content in quartz-bearing rocks: implications for hydrolytic weakening in the laboratory and within the earth. *Tectonophysics*, **172**, 255–271.

——, KIRBY, S. H., AINES, R. D. & ROSSMAN, G. R. 1986. Solubility and diffusional uptake of hydrogen in quartz at high water pressures: Implications for hydrolytic weakening. *Journal of Geophysical Research*, **91**, 12723–12744.

MACKWELL, S. J. & WEATHERS, M. S. 1987. The effects of fluid environment on the transport of metallic cations in quartzites. *EOS AGU Transactions* **68**, 1490.

——, LEE, V. W. & BRANTLEY, S. L. 1989. Fluid distribution in crustal rocks and effects on rheology. *28th International Geological Congress, Washington, abstracts vol. 2*, July 9–19, 1989, USA.

MAINPRICE, D. H. & PATERSON, M. S. 1984. Experimental studies of the role of water in the plasticity of quartzites. *Journal of Geophysical Research*, **89**, 4257–4269.

ORD, A. & HOBBS, B. E. 1986. Experimental control of the water weakening effect in quartz. *In*: HOBBS, B. E. & HEARD, H. C. (eds), *Mineral and Rock Deformation: Laboratory Studies*. Geophysical Monograph AGU, Washington, **36**, 51–72.

—— & —— 1987. The plastic deformation of quartz. *International Conference on Deformation of Crustal Rocks. Geological Society of Australia, Abstracts* **19**, 70–72.

PARRISH, D. K., KRIVZ, A. L. & CARTER, N. L. 1976. Finite-element folds of similar geometry. *Tectonophysics*, **32**, 183–207.

PATERSON, M. S. 1989. The interaction of water with quartz and its influence in dislocation flow—an overview. *In*: KARATO, S. & TORIUMI, M. (eds) *Rheology of Solids and of the Earth*. Oxford University Press, New York, N.Y., 107–142.

TULLIS, J., CHRISTIE, J. M. & GRIGGS, D. T. 1973. Microstructures and preferred orientations of experimentally deformed quartzites. *Geological Society of America Bulletin*, **84**, 297–314.

WATSON, E. B. & BRENAN, J. M. 1987. Fluids in the lithosphere, 1. Experimentally-determined wetting characteristics of CO_2-H_2O fluids and their implications for fluid transport, host-rock physical properties, and fluid inclusion formation. *Earth and Planetary Science Letters*, **85**, 497–515.

Received 5 March 1990; revised typescript accepted 16 July 1990.